CrossMark

Elaboration and characterization of glass–ceramic enriched by heavily manganese doped zinc silicate nanoparticles for optoelectronic applications

L. El Mir[1,2]

Abstract

Nanocrystallines Mn^{2+}-doped zinc silicate (β-Zn_2SiO_4:Mn) embedded in SiO_2 host matrix were synthesized in two steps. In the first one a sol–gel process was used for the elaboration of silica aerogel monolith enriched by ZnO:Mn nanoparticles using supercritical conditions of ethanol. In the second step a simple solid-phase reaction under natural atmosphere at 1500 °C was investigated. The structure and texture of the obtained nanocomposites were studied by X-ray diffraction and transmission electron microscopy respectively. The optical results indicate that the obtained nanocomposites have excellent luminescence properties in the visible range. In addition, the PL spectrum for the β-Zn_2SiO_4:Mn/SiO_2 nanocomposite reveals a band centered at about 584 nm attributed to the $^4T_1$–$^6A_1$ transitions of Mn^{2+} ions. The intensive yellow luminescence presents a red shift and the lifetime is relatively weak compared to the known luminescence properties of this material. The obtained results are attributed to the protocol used and the excess of Mn^{2+} ions. The linear diminishing behaviours of the PL integrate intensity with the operating temperature, and the variation of the time decay with the Mn^{2+} contents; make it possible to anticipate the utilization of this material in luminescence thermometry.

1 Introduction

Over the last decays, zinc silicate is becomes a perfect host material for transition metal ions in view of its chemical stability and transparency in the UV–Visible range [1–4]. Transition and rare-earth ions are superb luminescent centers because of their inner shell electronic transitions [5]. Thus, change and uncommon earth ion doped zinc silicates have been examined widely as potential luminescent materials [3–5]. In fact; it is notable that Zn_2SiO_4 is polymorphic material, including principally α, β phases. Zn_2SiO_4:Mn with α-phase is a stable structure and emits green radiation, while β-phase is a metastable structure which becomes stable only at very high synthesis temperature and displays yellow luminescence [6]. Numerous exploration works have been investigated on mixed oxides [7–12]. There are just a few reports on the preparation and analysis of β-Zn_2SiO_4:Mn powders [13, 14]. This is somewhat due to the non-stability of β-Zn_2SiO_4 which just forms under certain conditions [6]. For example, β-Zn_2SiO_4 was framed as a middle stage and changed into stable α-Zn_2SiO_4 under hydrothermal synthesis in supercritical conditions of water [15]. Moreover, the properties of β-Zn_2SiO_4 and process concerning yellow emission are as yet vague. In this paper, by appropriately designing and supercritical conditions of ethanol drying, we have effectively prepared β-Zn_2SiO_4:Mn nanoparticles embedded in silica matrix. The optical and physical properties of the as-prepared nanocomposite (β-Zn_2SiO_4:Mn/SiO_2) have been examined. Till now experimental work has been directed to α-Zn_2SiO_4:Mn and has been performed with sol–gel synthesis [16–19], polymer precursor methods [20], combustion synthesis [21], spray pyrolysis [22], chemical vapor deposition [23] and hydrothermal synthesis [24]. In any case, the nature of the nanoparticles with respect to size and size distribution are constrained; essential issues, like the level of agglomeration or the quantum yield have not been considered, yet. Morimo and Matea incorporated Zn_2SiO_4:Mn by sol–gel technique and compared the luminescence of their examples and those made by solid-state reactions [25]. They

✉ L. El Mir
Lassaad.ElMir@fsg.rnu.tn

1 Departement of Physics, College of Sciences, Al Imam Mohammad Ibn Saud Islamic University (IMSIU), Riyadh 11623, Saudi Arabia

2 Laboratory of Physics of Materials and Nanomaterials Applied at Environment (LaPhyMNE), Faculty of Sciences in Gabes, Gabes University, Gabès, Tunisia

obtained higher PL intensity for their examples containing 2% Mn loading. Li and collaborators have synthesized pure and Mn-doped zinc silicate utilizing different salts of zinc and found that the type of the precursor of the anion influences the morphology of the particles [26]. Later, Raynaud and colleagues built up an aqueous sol–gel protocol for silicate preparation, which gave α-Zn_2SiO_4 particle sizes of 1–3 μm with morphology very well-defined [27]. Be that as it may, up to now, the method for sol–gel preparation has utilized for the synthesis of the different nanocomposites where the silica used like a framework. Our target in this work is, in a first step the in-situ synthesis of luminescent nanoparticles of β-Zn_2SiO_4:Mn in a silica lattice whose goal is to expand the life of the sample and prevent contamination caused by the external environment. There is a need for more control over the shape, size, surface properties and purity of phosphors, which are compromised in high temperature synthesis. The luminescent properties of phosphors strongly depend on the crystal structure and particle size [28]. High temperature synthesis results in agglomeration of phosphor particles [28]. Further, crushing, ball milling, and grinding damage phosphor surfaces and decrease emission intensity [29].

Herein, we synthesized Mn-doped ZnO and Mn-doped β-Zn_2SiO_4 nanoparticles in SiO_2 host matrix with high Mn^{2+} loading. In order to give more stability for potential applications to our samples; particular elaboration process was adopted based on sol–gel route followed by furnace firing at 1500 °C for 2 h. The crystalline properties, PL emission spectra, and decay time were systematically studied.

2 Experimental procedure

2.1 Preparation of β-Zn_2SiO_4:Mn nanocomposites

The preparation of colloid suspension particles in silicate network has been done in three stages. In the first one, nanoparticles of ZnO:Mn aerogels, with high atomic manganese doping concentration of [Mn]/([Zn]+[Mn]) = 20%, have been realized by a modified sol–gel technique according to El Mir et al. approach [6]. In this process, nanocrystalline ZnO:Mn aerogels were synthesized by dissolving 4 g of zinc acetate dehydrate (Zn(CH_3COO)·$2H_2O$) and adequate quantity of manganese (II) chloride-4-hydrate ($MnCl_2·4H_2O$) in 14 ml of methanol under magnetic stirring for 2 h. The water for hydrolysis was slowly released by esterification reaction of acetone with methanol to control the size of the formed nanoparticles. The drying was realized in autoclave under supercritical conditions of ethyl alcohol (EtOH). In the second stage, we have synthesized ZnO:Mn dispersed in silica aerogel as indicated by the following procedure: 1 ml of tetraethylorthosilicate (TEOS) was first dissolved in EtOH.

At that point, with steady mixing of the blend of TEOS and EtOH, 0.88 ml of water and 60 mg of nanoparticles powder as obtained in the initial step were added. The entire solution was mixed for around 30 min, bringing to the development of a uniform sol. After, the obtained sol was moved to tube in ultrasonic bath where 100 ml of fluoride acid (HF) was added. The wet gel was obtained in some seconds. White and monolithic aerogel was acquired by supercritical drying in EtOH as portrayed in the initial step. At long last, glass–ceramic containing β-$Zν_2SiO_4$:Mn particles were gotten after thermal treatment of the aerogel at 1500 °C for 2 h. The used processes are summarized in Table 1.

2.2 Characterization

The crystalline phases of our samples were identified by X-ray diffraction (XRD) using a Bruker D5005 powder X-ray diffractometer using a CuKα source (1.5418 Å radiation). Crystallite sizes (G, in Å) were estimated from the Scherrer's equation (Eq. 1) [30]:

$$G = \frac{0.9\lambda}{B\cos\theta_B} \tag{1}$$

where λ is the X-ray wavelength (1.5418 Å), θ_B is the maximum of the Bragg diffraction peak (in radians) and B is the linewidth at half maximum. Transmission electron microscopy (TEM, JEM-200CX) was used to study the morphology and particle size of the phosphor powders. The specimens for TEM were prepared by putting the as-grown products in EtOH and immersing them in an ultrasonic bath for 15 min, then dropping a few drops of the resulting suspension containing the synthesized materials onto TEM grid. The elemental mapping image and EDS were performed by (FE-SEM, JEOL JSM-7800F) field-emission scanning electron microscopy. For photoluminescence (PL) measurements, a laser 337.1 line of Laser Photonics LN 100 nitrogen and 450-W Xenon lamp were used as an excitation sources. The emitted light from the sample collected by an optical fiber on the same side as the excitation was analyzed with a Jobin–Yvon Spectrometer HR460 and a multichannel CCD detector (2000 pixels). The photoluminescence excitation (PLE) measurements were performed on a Jobin–Yvon Fluorolog 3–2 spectrometer. The decays were analyzed by a

Table 1 Synthesis processes and conditions

Synthesis product	Process	Synthesis temperature (C)
ZnO:Mn	Sol–gel	250
β-Zn_2SiO_4:Mn/SiO_2	Sol–gel followed by solid reaction	1500

PM Hamamatsu R928 and a scope Nicolet 400 with a time constant of the order of 1 ns. The low temperature experiments were carried out in a Janis VPF-600 Dewar with variable temperature controlled between 78 and 300 K.

3 Results and discussion

3.1 Structural and mophological studies

Figure 1 depicts the XRD patterns of Mn doped-ZnO nanopowder. The strongest peaks were observed at $2\theta = 31.664°$, $34.395°$ and $36.293°$ corresponding to those of pure zinc oxide. All the diffraction peaks could be fitted with the hexagonal wurtzite structure. The obtained data is in well agreement with the Joint Committee on Powder Diffraction Standards (JCPDS) card no JCPDS PDF no 36-1451 [16]. Globally, the peak positions shift to smaller angles compared to undoped zinc oxide ones prepared in the same conditions, because of the increase in the inter-planar spacing due to substitution of lattice site by an ion of higher radius [31]. There is a slight increase in lattice parameter values for Mn doped-ZnO nanocrystalline particles (for Mn doped-ZnO: a = 3.251 Å, c = 5.207 Å) compared to that of ZnO sample (a = 3.249 Å, c = 5.205 Å, JCPDS no. 36-1451). The increased lattice parameter values of Mn doped-ZnO indicate the incorporation of manganese in zinc oxide particles [31]. The ionic radius of Zn^{2+} (~0.60 Å) is smaller than Mn^{2+} (~0.67 Å) ions [32]. In the case of high doping concentration by Mn, excessive doping usually resulted in segregation of secondary phase in grain boundaries, which may involve poor crystallinity [33, 34].

The large difference between the real Mn concentration and the nominal Mn concentration is understandable because partial raw materials remain in the reaction solution. Mn^{2+} ions have a solid solubility limit of about 13–25% in ZnO matrix depending on synthesis technique [35]. When the real Mn concentration of the sample with a nominal Mn concentration is in order of the solid solubility limit the Mn ions were easily diluted in the ZnO host matrix. In other hand, according to Scherrer's formula (Eq. 1) and after a correction for the instrumental broadening, the grain size value of the crystallites was estimated of about 40–50 nm.

Figure 2 shows the X-ray diffraction patterns of β-Zn_2SiO_4/SiO_2 glass–ceramic nanocomposite treated at 1500 °C for 2 h in air. It is clear that all the diffraction peaks are in good agreement with those of the standard pattern reported by the Joint Committee on Power Diffraction Standard (JCPDS No. 19-1479) [4, 5]. After the incorporation of these nanoparticles of ZnO:Mn in SiO_2 and thermal treatment at high temperature, a new zincic phase (β-Zn_2SiO_4) was formed in-situ of glass matrix. In our results the pattern resembles to that of β-$Z\nu_2SiO_4$, with slightly difference in the peak position and the number of peaks to the results reported by Roobsky and McKeag [4]. The above results imply that the solid reaction between ZnO and SiO_2 occurred to form the β-$Z\nu_2SiO_4$ phase during heat treatment at 1500 °C. It is clear that the most dominant crystalline phase corresponds to the β-Zn_2SiO_4 phase, in parallel we note the appearance of two other phases of silica [4, 13]. However, at high temperature, Zn^{2+} and Si^{2+} species in the structure appear to be mobile enough to move and diffuse inside the porous body and contribute to the formation of β-$Z\nu_2SiO_4$ phase. Nevertheless, we do not find any diffraction about Mn^{2+} ion compound, which indicates that Mn^{2+} ions entered into the lattice of β-$Z\nu_2SiO_4$. The average grain size of the crystallites Zn_2SiO_4 in our samples is about 70 nm [13], has been estimated using Scherrer's formula (Eq. 1).

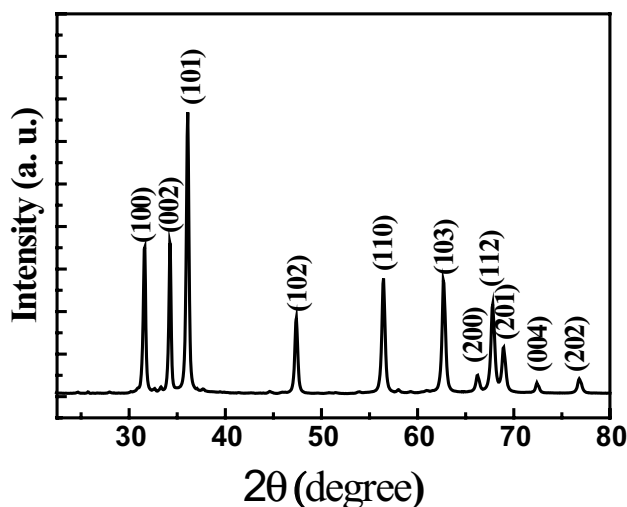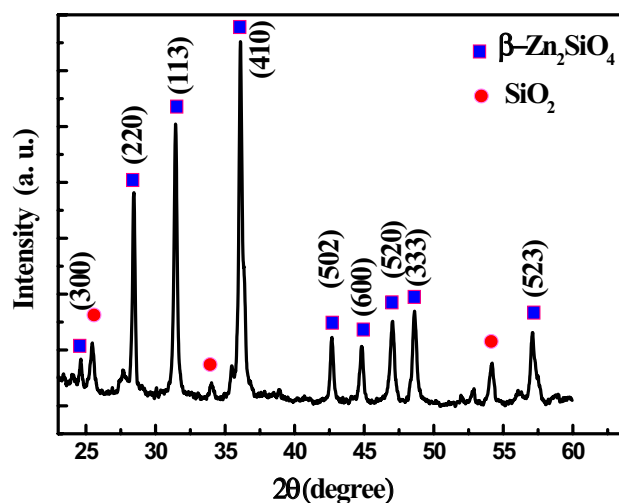**Fig. 1** X-ray diffraction pattern of the ZnO:Mn nanopowder

**Fig. 2** X-ray diffraction pattern of the β-Zn_2SiO_4:Mn nanocomposite

We investigated the size and morphology of our samples by transmission electron microscopy. The TEM image of Mn-doped ZnO nanoparticles (Fig. 3a) shows that very small ZnO particles are present in the as-prepared aerogel powder. The size of the majority of ZnO:Mn particles in this powder vary between 40 and 50 nm. Taking into account the results of crystallite size measurements by XRD, it can be concluded that the crystallite size is approximately equal to the particle size in the powder prepared in the present work.

The TEM micrographs of the β-Zn_2SiO_4:Mn/SiO_2 glass–ceramic (Fig. 3b) indicating that the presence of Zn_2SiO_4 nanoparticles dispersed in the silica matrix. At high annealing temperature of 1500 °C for two hours, Zn and Si species move and diffuse inside the porous body to form β-$Zν_2SiO_4$ phase. For that reason we illustrated the enhancement of the particle size which increases from about 40 nm for ZnO:Mn to 70 nm for Zn_2SiO_4. Figure 3c shows the elemental mapping sum image of the β-Zn_2SiO_4:Mn/SiO_2 glass–ceramic sample. Non homogenous dispersion of the different elements was illustrated. This behavior is well explained by physiological nature of our nanocomposite. Energy dispersive spectroscopy (EDX) analysis, shown in Fig. 3d, confirms the presence of manganese (Mn), in good agreement with XRD and elemental mapping sum image results.

3.2 Optical properties

Figure 4 shows the photoluminescence emission intensities at different measurement temperatures of β-Zn_2SiO_4:Mn/SiO_2 glass–ceramic, synthesized by sol–gel method followed by furnace firing at high temperature (1500 °C for 2 h) using El Mir et al. protocol [36, 37], under UV excitation. The yellow emission has been assigned to $^4T_1(^4G) \rightarrow {}^6A_1(^6S)$ electronic transition, peaking at the wavelength 584 nm and which is a parity forbidden emission transition of Mn^{2+} ions [13]. The diagram demonstrates that the relative PL power increments when the measure temperature decreases. This emission centered at 584 nm, corresponds to the energy transfer in the Mn^{2+} ions [13]. With Mn^{2+} occupies part of the Zn^{2+} sites, which is tetra-coordinated by four oxygen atoms [5, 13]. The crystal field around Mn^{2+} ions involves a low splitting width of its 3d energy levels, in accordance with the perceptions of Barthou et al. [36]. As a result, an intensive yellow emission at 584 nm is obtained with noteworthy red-shift compared to the luminescence generally obtained with low Mn^{2+} loading [38–41]. Also, a noticeable red-shift of the PL emission band with the enhancement of the measurement temperature was observed; this is generally explained by the exchange interactions between Mn^{2+} ions [42]. In Zn_2SiO_4 phase, the Mn^{2+} ions are arranged at the marginally distorted tetrahedral sites with four oxygen

Fig. 3 Morphology and chemical elementary analysis of the samples. **a** TEM of ZnO:Mn, **b** TEM of the nanocomposite, **c** EDX analysis of the ZnO:Mn, **d** EDX analysis of the nanocomposite. (Color figure online)
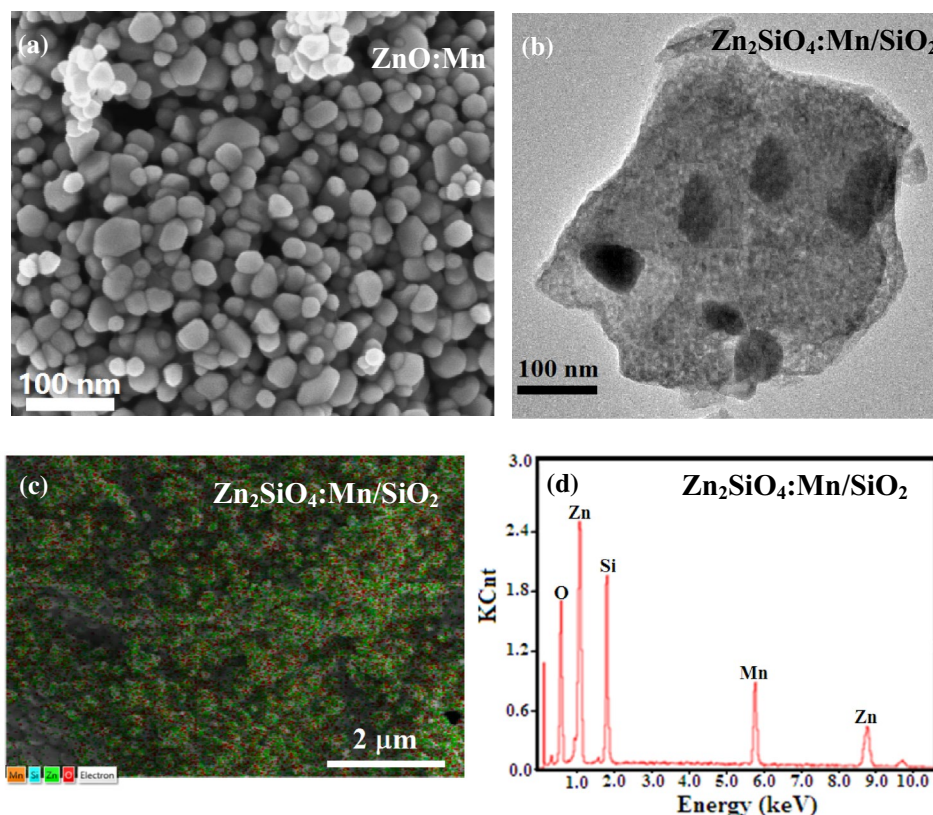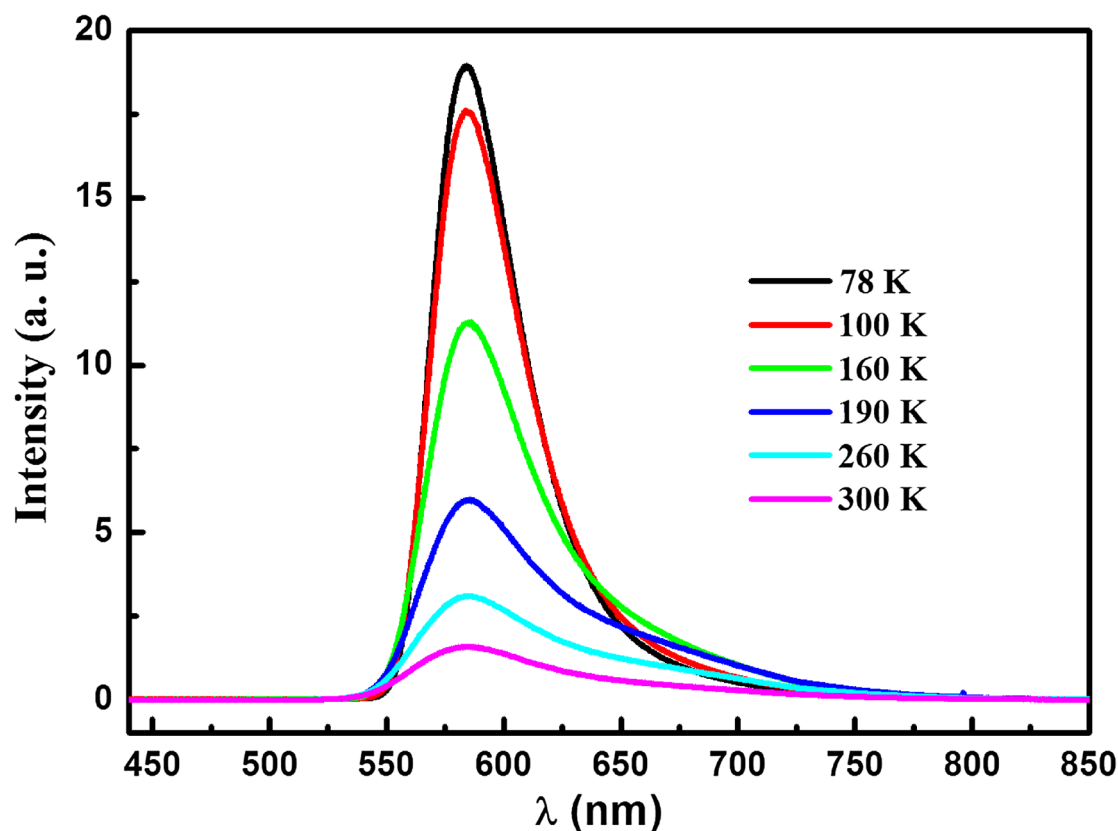
Fig. 4 PL spectra of the β-Zn$_2$SiO$_4$:Mn nanocomposite at different temperatures. (Color figure online)

neighbors [42]. The used wavelength of excitation of 255 nm corresponding to photon energy of 4.86 eV is smaller than the band gap energy of Zn$_2$SiO$_4$. The excitation of Mn^{2+} ions follows their ionization i.e., the transition from the ground state to the conduction band, and the non-radiative relaxation of the electrons to the excited state $^4T_1$ of Mn^{2+} [13]. From the PL spectrum, a slight red-shift of the maximum of the peak is denoted while the emission intensity enhances. It is known that the internal luminescence of the Mn^{2+} ion is influenced the host crystal field. Mn^{2+} ions in the Zn$_2$SiO$_4$ host matrix with higher crystallinity feel an intensive crystal field. An increase of this field reduces the energy difference of the ground and the first excited state, inducing a peak broadening so a small red-shift of the emission peak [43]. Furthermore, the area of the sub yellow-discharge band at 584 nm versus the measurement temperatures is depicted in Fig. 5. These integrate intensity declined markedly as the temperatures expanded. The intensive yellow luminescence presents a red shift compared to previous works [38–40] where the luminescence was observed at about 570 nm; this result is principally due to the used protocol consisting on the in-situ synthesis of the zinc silicate phase and the high Mn^{2+} loading. On the other hand, the excitation spectrum of β-Zn$_2$SiO$_4$:Mn/SiO$_2$ glass–ceramic comprises a strong
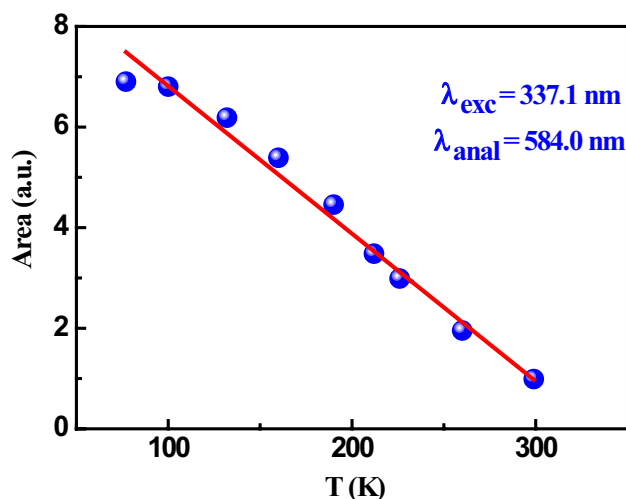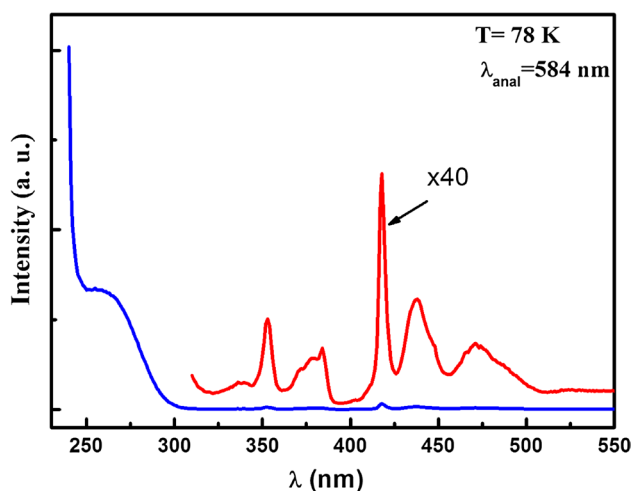

Fig. 5 Area the sub yellow-emission band (584 nm) a function of different temperatures. (Color figure online)

excitation band extending from 220 to 300 nm with a most extreme at 255 nm, which is attributed to excitation of Mn^{2+} charge transfer transition [18] (Fig. 6). The spectrum shows a broadband intense peak, which is corresponds to the charge
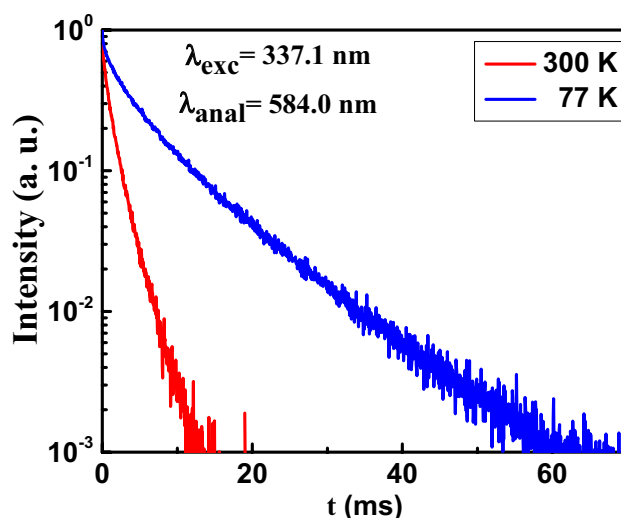
Fig. 6 PLE spectra of the β-Zn$_2$SiO$_4$:Mn nanocomposite

Fig. 7 Decay curve of the β-Zn$_2$SiO$_4$:Mn nanocomposite at different measurement temperature. (Color figure online)

transfer (CT) band of Mn^{2+} in the Zn$_2$SiO$_4$ phase as ascribed by Mishra et al. [44]. Likewise, to the CT band, additional bands of Mn^{2+} (d–d) transition are also seen at higher wavelengths; these are caused by the splitting of the ^{4}D and ^{4}G levels in view of the crystal field, as presented in the Orgel diagram for Mn^{2+} [41, 45, 46]. The electrons at the ground state ^{6}A$_1$(^{6}S) of Mn^{2+} ions, which originate from the photoexcited ionization of Mn^{2+}, are excited by photons to the Zn$_2$SiO$_4$ conduction band, and the obtained free electrons in the conduction band relax back to the ^{4}T$_1$(^{4}G) excited state through a non-radiative process [47]. At last, this is trailed by radiative transition from the ^{4}T$_1$(^{4}G) excited state to the ^{6}A$_1$(^{6}S) ground state, emitting visible light at 584 nm. This happens when Mn ions occupy the tetrahedral sites of the triclinic system. It can likewise clarify the motivation behind why warm treatment of the samples at high temperature at around 1500 °C is generally important for the development of β-Zν_2SiO$_4$:Mn/SiO$_2$ nanocomposite, since Zn^{2+} and Mn^{2+} ions are probably going to move to bigger interstices more than tetrahedral ones, to settle them in such bigger interstices instead to returning to tetrahedral interstices [38]. Moreover, the distinction in the coordination condition might be the origin of the red-shift of Mn emission in Zn$_2$SiO$_4$:Mn/SiO$_2$ glass–ceramic nanocomposite [2].

The yellow emission decays at 584 nm of the sample at different measurement temperatures 78 K and 300 K are shown in Fig. 7. The curves show that the decay kinetics are exponential; so the result can be obtained according to the following equation (Eq. 2) [1]:

$$I = Ae^{(-t/\tau)} \tag{2}$$

where τ is the luminescent lifetime and A is the pre-exponential factor. From the fitting results we get A = 0.98, τ = 0.6 ms at 300 K, while in the case of 78 K we found τ = 3 ms. This trend is in agreement with the previous

observations but for green emission for the same material prepared at lower temperature of about 1200 °C [38]. The long decay time of Zn$_2$SiO$_4$:Mn is a snag for the PDP application. Along these lines, parcel of endeavors have been devoted to reduce the decay time of Zn$_2$SiO$_4$:Mn materials without losing its interesting efficiency [15, 38]. It is conceivable to reduce the time decay of the phosphor material by expanding the dopant content. In any case, on account of the accompanying energy transfer, non-radiative de-excitation procedures will increment and the sample efficiency will diminish because of the well-known high loading dopant effect. At the point when the dopant loading is enhanced, the opposition effect between a higher number of excited centers and lower radiative efficiency will decide the ideal dopant content [38]. Morell and Khiati [45] attributed such behavior to quenching effect. More recently Barthou et al. [38] found that there exist two different activation centers with different decay time and that the faster one is predominant at high Mn concentration, which is believed to be Mn–Mn pairs in Zn$_2$SiO$_4$.

4 Conclusion

ZnO:Mn nanoparticles and β-Zn$_2$SiO$_4$:Mn/SiO$_2$ glass–ceramic nanocomposite have been synthesized by sol–gel technique. The X-ray diffraction and TEM of Mn-doped ZnO nanoparticles show a crystalline phase with a particle size ranging between 40 and 50 nm. Upon incorporation of ZnO:Mn nanoparticles in SiO$_2$ and heat treatment at 1500 °C, β-Zn$_2$SiO$_4$ phase was formed in-situ of SiO$_2$ host matrix. The obtained sample showed a strong promising yellow luminescence. From the analysis of the PL and

PLE spectra, it can be concluded that the luminescence band at 584 nm can be attributed to Mn^{2+} in β-Zn_2SiO_4 phase. The advantages of this method include simplified procedure, low cost, large-scale production and controlled lifetime by doping concentration, which have potential applications in lighting fields and optoelectronic devices.

References

1. R. Selomulya, S. Ski, K. Pita, C.H. Kam, Q.Y. Zhang, S. Buddhudu, Mater. Sci. Eng. B **100**, 136 (2003)
2. L. El Mir, A. Amlouk, C. Barthou, J. Phys. Chem. Solids **67**, 2395 (2006)
3. H. Wang, Y. Ma, G. Yi, D. Chen, Mater. Chem. Phys. **82**, 414 (2003)
4. H.P. Rooksby, A.H. McKeag, Trans. Faraday Soc. **37**, 308 (1941)
5. M. Mai, C. Feldmann, J. Solid State Sci. **11**, 528 (2009)
6. L. El Mir, K. Omri, J. El Ghoul, A.S. AL-Hobaib, H. Dahman, C. Barthou, Superlattices Microstruct. **65**, 248 (2014)
7. M. Eghbali-Arani, A. Sobhani-Nasab, M. Rahimi-Nasrabadi, S. Pourmasoud, J. Mater. Sci. **47**, 3757 (2018)
8. S.S. Hosseinpour-Mashkani, A. Sobhani-Nasab, J. Mater. Sci. **28**(21), 16459 (2017)
9. M. Salavati-Niasari, F. Soofivand, A. Sobhani-Nasab, M. Shakouri-Arani, M. Hamadanian, S. Bagheri, J. Mater. Sci. **28**(20), 14965 (2017)
10. A. Sobhani-Nasab, A. Ziarati, M. Rahimi-Nasrabadi, M.R. Ganjali, A. Badiei, Res. Chem. Intermed. **43**(11), 6155 (2017)
11. M.E. Arani, A. Sobhani-Nasab, M. Rahimi-Nasrabadi, F. Ahmadi, S. Pourmasoud, Ultrason. Sonochem. **43**, 120 (2018)
12. A. Sobhani-Nasab, M. Rahimi-Nasrabadi, H.R. Naderi, V. Pourmohamadian, F. Ahmadi, M.R. Ganjali, H. Ehrlich, Ultrason. Sonochem. **45**, 189 (2018)
13. Y. Jiang, J. Chen, Z. Xie, L. Zheng, J. Mater. Chem. Phys. **120**, 313 (2010)
14. B. Li, J. Zhou, R. Zong, M. Fu, L. Li, Q. Li, J. Am. Ceram. Soc. **89**, 2308 (2006)
15. M. Takesue, K. Shimoyama, K. Shibuki, A. Suino, Y. Hakuta, H. Hayashi, Y. Ohishi, R.L. Smith Jr., J. Supercrit. Fluids **49**, 351 (2009)
16. K. Omri, J. El Ghoul, A. Alyamani, C. Barthou, L. El, Mir, Physica E **53**, 48 (2013)
17. J. El Ghoul, K. Omri, A. Alyamani, C. Barthou, L. El Mir, J. Luminesc. **138**, 218 (2013)
18. J.El Ghoul, C. Barthou, M. Saadoun, L.El Mir, J. Physica B **405**, 597 (2010)
19. J. El Ghoul, K. Omri, L. El Mir, C. Barthou, S. Alaya, J. Luminesc. **132**, 2288 (2012)
20. Q. Bin, Z.L. Tang, Z.T. Zhang, X.X. Wang, Rare Metal Mater. Eng. **32**, 711 (2003)
21. A. Manavbasi, J.C. LaCombe, J. Mater. Sci. **42**, 252 (2007)
22. Y.C. Kang, H.D. Park, Appl. Phys. A **77**, 529 (2003)
23. A. Roy, S. Polarz, S. Rabe, B. Rellinghaus, H. Zahres, F.E. Kruis, M. Driess, Chem. Eur. J. **10**, 1565 (2004)
24. H.F. Wang, Y.Q. Ma, G.S. Yi, D.P. Chen, Mater. Chem. Phys. **82**, 414 (2003)
25. R. Morimo, K. Matae, Mater Res Bull. **24**, 175 (1989)
26. Q.H. Li, S. Komaraneni, R. Roy, J. Mater. Sci. **30**, 2358 (1995)
27. L. Reybaud, C. Broca-Cabarreq, A. Mosset, H. Ahamdane, Mater. Res. Bull. **31**, 1133 (1996)
28. H.-K. Jung, D.-S. Park, Y.C. Park, Mater. Res. Bull. **34**, 43 (1999)
29. I.F. Chang, J.W. Brownlow, T.I. Sun, J.S. Wilson, J. Electrochem Soc. **136**, 3532 (1989)
30. B.D. Cullity, *Elements of X-ray Diffractions* (Addison-Wesley, Reading, 1978)
31. S. Karamat, S. Mahmood, J.J. Lin, Z.Y. Pan, P. Lee, T.L. Tan, S.V. Springhama, R.V. Ramanujan, R.S. Rawat, Appl. Surf. Sci. **254**, 7285 (2008)
32. K.P. Bhatti, S. Chaudhary, D.K. Pandya, S.C. Kashyap, Solid State Commun. **136**, 384 (2005)
33. J. Han, P. Mantas, A. Senos, J. Eur. Ceram. Soc. **20**, 2753 (2000)
34. K.K. Nagaraja, S. Pramodini, A. Santhosh Kumar, H.S. Nagaraja, P. Poornesh, D. Kekuda, Opt. Mater. **35**, 431 (2013)
35. Y.Q. Chang, D.B. Wang, X.H. Luo, X.Y. Xu, X.H. Chen, L. Li, C.P. Chen, R.M. Wang, J. Xu, D.P. Yu, Appl. Phys Lett. **83**, 4020 (2003)
36. L. El Mir, A. Amlouk, C. Barthou, S. Alaya, J. Physica B **388**, 412 (2007)
37. L.El Mir, J. El Ghoul, S. Alaya, M. Ben Salem, C. Barthou, H.J. von Bardeleben, Physica B **403**, 1770 (2008)
38. C. Barthou, J. Benoit, P. Benalloul, A. Morell, J. Electrochem. Soc. **141**, 524 (1994)
39. , K. Omri, Superlattices Microstruct. **55**, 89 (2014)
40. K. Omri, O.M. Lemine, L. El Mir, Ceram. Int. **43**, 6585 (2017)
41. K. Omri, A. Alyamani, L.El Mir, Appl. Phys. A **124**, 215 (2018)
42. S. Dembski, S. Ruppa, M. Milde, C. Gellermann, M. Dyrba, S. Schweizer, M. Batentschuk, A. Osvet, A. Winnacker, J. Opt. Mater. **33**, 1106 (2011)
43. X. Li, F. Chen, Mater. Res. Bull. **48**, 2304 (2013)
44. K.C. Mishra, K.H. Johnson, B.G. DeBoer, J.K. Berkowitz, J. Olsen, E.A. Dale, J. Lumin. **47**, 197 (1991)
45. A. Morell, N. El Khiati, J. Electrochem. Soc. **140**, 2019 (1993)
46. L.E. Orgel, J. Chem. Phys. **23**, 1004 (1955)
47. L. Xiong, J. Shi, J. Gu, L. Li, W. Huang, J. Gao, M. Ruan, J. Phys. Chem. B **109**, 731 (2005)